Neoplasma 2025; 72(1–2): 91–105

doi:10.4149/neo_2025_250110N13

# IL4I1 knockdown inhibits the epithelial-mesenchymal transition process in glioma via downregulation of the JAK2/STAT3 signaling pathway

Jianwei ZHUO[1,2,#], Tong WANG[1,#], Ting LU[1], Xiangying LI[1], Zhengquan YU[1], Gang CUI[1,*], Haitao SHEN[1,*]

[1]*Neurosurgery & Brain and Nerve Research Laboratory, The First Affiliated Hospital of Soochow University, Suzhou, Jiangsu, China;* [2]*Department of Neurosurgery, The Fourth People's Hospital of Taizhou, Taizhou, Jiangsu, China*

**Correspondence: CG_neurosurgery@163.com; shenhaitao1990@suda.edu.cn*
*[#]Contributed equally to this work.*

**Received January 10, 2025 / Accepted April 9, 2025**

Gliomas are primary intracranial tumors that cause considerable morbidity and mortality. The effect of interleukin 4-induced gene-1 (IL4I1) on the progression of various diseases has been demonstrated to be significant. However, the specific molecular mechanisms of how IL4I1 contributes to the progression and the epithelial-mesenchymal transition (EMT) process of glioma remain inadequately elucidated. IL4I1 expression in glioma was assessed using public datasets and immunohistochemistry. In *in vitro* experiments, IL4I1 expression was quantified through real-time quantitative PCR and western blotting. The effects of IL4I1 knockdown on the malignant phenotypes of glioma cells were investigated through *in vitro* studies. The evaluation of biomarkers associated with EMT and the Janus-activated kinase 2/signal transducer and activator of transcription 3 (JAK2/STAT3) pathway was conducted using western blotting and immunofluorescence assays after IL4I1 knockdown. A xenograft tumor model was established to validate the influence of IL4I1 knockdown in glioma progression. The results revealed that high expression of IL4I1 is linked to an unfavorable prognosis in human gliomas. IL4I1 knockdown effectively impeded the malignant phenotypes of glioma cells. IL4I1 knockdown induced EMT reversal, characterized by alterations in the expression levels and localization of EMT-related biomarkers. This reversal is partially mediated through the JAK2/STAT3 signaling pathway. The results of in vivo experiments confirmed that IL4I1 knockdown effectively suppressed glioma growth. Our research demonstrates that IL4I1 knockdown reverses the EMT process via JAK2/STAT3 signaling pathway and suppresses the malignant phenotypes of glioma, thereby highlighting its potential as both a prognostic marker and therapeutic target for glioma.

*Key words: IL4I1; glioma; JAK2/STAT3; EMT; knockdown*

Glioma, particularly glioblastoma multiforme (GBM), is a highly prevalent and fatal primary intracranial tumor characterized by unfavorable prognosis and rapid progression [1, 2]. Despite advancements in surgical, chemotherapeutic, and radio-therapeutic interventions, the average duration of survival for individuals diagnosed with GBM stands at 14.6 months [3]. It is essential to comprehensively explore the molecular mechanism of glioma to identify more effective molecular targets for it.

The nomenclature of interleukin 4-induced gene-1 (IL4I1) originates from the discovery of its mRNA in mouse B splenocytes. Situated within the leukocyte-receptor complex on chromosome 19, the IL4I1 gene encodes a glycosylated protein [4]. The authors of previous studies on IL4I1 initially focused on its involvement in immune response [5, 6]. A mounting body of evidence has elucidated the substantial role of IL4I1 in diverse tumorigenesis [7–9]. The role of IL4I1 in glioma has not been extensively studied, limited available evidence suggests its potential involvement in tumor progression and immune modulation. A multi-database analysis of the tryptophan metabolic gene in glioma suggested that IL4I1 may function as an oncogene and is associated with poor prognosis in patients [10]. Another study demonstrated that IL4I1 expression is elevated in glioma at both the transcriptome and protein levels, contributing to M2-like macrophage polarization and the enhancement of glioma cell invasiveness and motility [11]. Taken together, these studies provide evidence supporting further in-depth investigations into the mechanistic and clinical relevance of IL4I1 in glioma.

Epithelial-mesenchymal transition (EMT) is an intricate and ever-evolving cellular phenomenon characterized by substantial phenotypic plasticity, which plays a critical role

Copyright © 2025 The Authors.
This article is licensed under a Creative Commons Attribution 4.0 International License, which permits use, sharing, adaptation, distribution, and reproduction in any medium or format, as long as you give appropriate credit to the original author(s) and the source and provide a link to the Creative Commons licence. To view a copy of this license, visit https://creativecommons.org/licenses/by/4.0/

in tumor development [12, 13]. Its activation reduces cellular adhesion and polarity, which facilitates invasive expansion and metastasis of tumors. Of late, the existence of an EMT process in central nervous system tumors has become widely accepted [14, 15]. The complex progression of EMT in gliomas involves the regulation of various molecular mechanisms, including the Notch and Wnt/β-catenin pathways [14, 16]. Emerging evidence suggests that signal transducer and activator of transcription 3 (STAT3), a crucial player in cancer development, induces EMT through the Janus-activated kinase 2 (JAK2)/STAT3 signaling pathway [17, 18].

In the study presented herein, we conducted an analysis of the IL4I1 expression profile in gliomas and its association with clinical and pathologic characteristics. We conducted cell and molecular biology experiments to determine the effect of IL4I1 knockdown on glioma malignant phenotypes and the EMT process. To investigate the mechanisms underlying IL4I1 knockdown-mediated EMT, we explored the possible involvement of the JAK2/STAT3 signaling pathway. Lastly, in an *in vivo* setting, we performed xenograft assays to assess the impact of IL4I1 on glioma proliferation and growth. These findings demonstrate the importance of IL4I1 in glioma and provide a novel target for glioma therapy.

## Patients and methods

**Database acquisition.** The clinical and RNA sequencing data of patients examined in the present study were acquired from the publicly accessible Chinese Glioma Genome Atlas (CGGA) database (http://www.cgga.org.cn/) and The Cancer Genome Atlas (TCGA) database (https://tcga-data.nci.nih.gov/tcga/). The 325 glioma samples from CGGA and 702 glioma samples from TCGA cohorts were divided into high- and low-expression groups according to the median IL4I1 expression levels.

**Human tissue sample collection.** From 2016 to 2022, 76 glioma specimens were surgically excised and pathologically examined at the First Affiliated Hospital of Soochow University. Additionally, eight brain samples without tumors were obtained from patients who underwent traumatic brain injury or intracerebral hemorrhage, necessitating the removal of a minute fraction of their brain tissues to alleviate intracranial pressure and enhance therapeutic efficacy. After fixation in 4% paraformaldehyde (PFA), the tissue samples were subjected to histological assays. Neither radiotherapy nor chemotherapy had been administered to the glioma patients prior to the tumor resection procedures. Informed consent was obtained from all individual participants included in the study. The ethics committee of the First Affiliated Hospital of Soochow University approved the experimental protocols (No. 2024480).

**Cell culture and treatment.** The Cell Bank of Shanghai Institutes for Biological Science (Shanghai, China) provided a selection of human glioma cell lines: U138, A172, U87, T98, U251, U118, U343, and the human astrocyte cell line HA 1800. The glioma cells were grown in Dulbecco's modified Eagle medium (DMEM) (KeyGEN, Nanjing, China), supplemented with 10% fetal bovine serum (FBS) (Biological Industrie, Kibbutz Bet-Haemek, Israel) and maintained at 37 °C with 5% $CO_2$. The HA 1800 cells were cultured in a specialized medium designed for astrocytes (KeyGEN). For the rescue experiment, glioma cells were exposed to a concentration of 20 μM of RO8191 (Sigma, St. Louis, USA), an activator of the JAK2/STAT3 pathway [19].

**Cell transfection.** Stable IL4I1 knockdown was achieved by using lentiviral particles containing IL4I1 short hairpin (sh) RNA purchased from Genechem Biotechnology Company (Shanghai, China). The specific sequences for IL4I1 knockdown were as follows: sh#1-IL4I1: 5'-CGGCCACCAAGGTGTTCCTAA-3'; sh#2-IL4I1: 5'-CACACGCTCTTGGAATATCTT-3'; sh#3-IL4I1: 5'-GCGCAACTATGTGGTGGAGAA-3'. IL4I1-specific shRNA was transfected into the cells (A172 and U138) based on the manufacturer's protocols using HitransG transfection reagent (Genechem). Cells that had undergone stable transfection were chosen by subjecting them to treatment with 2 μg/ml of puromycin. In order to evaluate any non-specific effects of transfection, the cells were transfected with scrambled shRNA lentiviral particles (Genechem) and referred to as "negative control (sh-Ctrl)" for comparative purposes. After transfection, the cells were kept at 37 °C for 48 h. Transfection efficiency was crudely surpassed 80%, as assessed with the green fluorescent protein (GFP).

**Real-time quantitative polymerase chain reaction (RT-qPCR).** RNA was isolated from the cells using TRIzol reagent (Invitrogen, Carlsbad, USA), followed by quantification using a Nanodrop spectrophotometer (ThermoScientific, Waltham, USA). All RNA samples exhibited a 260/280 nm ratio ranging from 1.9 to 2.0, indicating purity. Subsequently, the obtained RNA was subjected to reverse transcription by utilizing a cDNA Synthesis Kit (ThermoScientific) in a reaction volume of 20 μl with 1 μg of RNA sample. For PCR amplification, PowerUp SYBR Green Master Mix (Invitrogen) was utilized following the manufacturer's guidelines. The amplification primers were synthesized by GeneScript Biological Science and Technology (Nanjing, China). The PCR primers used in this study were designed with the following sequences: IL4I1-F 5'-ACTCGCCCGAAGACATCTAC-3'; IL4I1-R 5'-CATCCTCGGACATCACGTCTC-3'; GAPDH-F 5'-CAGGAGGCATTGCTGATGAT-3'; GAPDH-R 5'-GAAGGCTGGGGCTCATTT-3'. GAPDH was used as a reference. The results were determined by utilizing the $2^{-\Delta\Delta CT}$ approach.

**Western blotting (WB).** Total protein and membrane protein from cells were extracted using a whole cell lysis assay (Beyotime, Shanghai, China) and a membrane protein extraction kit (Bestbio, Shanghai, China), respectively. The loading buffer was mixed with the protein samples and then subjected to sodium dodecyl sulfate-polyacrylamide gel electrophoresis for separation. Following transfer to a nitrocellulose membrane, the proteins were blocked for 1 h with a

5% bovine serum albumin (BSA) solution (Amresco, Solon, USA). Incubation of primary antibodies continued overnight, and the nitrocellulose membranes underwent incubation with horseradish peroxidase (HRP)-linked anti-rabbit/mouse secondary antibodies (1:3,000; Proteintech, Wuhan, China) for 1 h. The blots were observed via chemiluminescence (ThermoScientific) and captured with a Chemiluminescent Western Blot Scanner (Gene Company, Hong Kong, China). GAPDH, tubulin, and $Na^+/K^+$-ATPase were used as endogenous references, as appropriate for each case. Band quantification was executed using ImageJ software (v1.51j8; National Institutes of Health, Bethesda, USA). The primary antibodies used are detailed in Supplementary Table S1.

**Cell proliferation assay.** In the cell counting kit-8 (CCK-8) assay, cells ($4\times10^3$/well) were distributed into a 96-well plate. The CCK-8 reagent (Beyotime) was introduced into each well after 24, 48, and 72 h, followed by incubation for 2 h. Absorbance was then measured at 450 nm. The cells ($3\times10^4$/well) were seeded into a 24-well plate and left to incubate overnight for the 5-ethynyl-2'-deoxyuridine (EdU) assay. The cells were treated with EdU (Beyotime) for 2 h. Subsequently, they were fixed using 4% PFA for 15 min and permeabilized utilizing 0.3% Triton X-100 (Beyotime) for another 15 min. The cells were exposed to the Click Reaction Mixture from the EdU staining kit and incubated for 30 min while avoiding exposure to light. The cells were subsequently stained using 4',6'-diamidine-2'-phenylindole dihydrochloride (DAPI) (Beyotime). Thereafter, microscopic imaging was performed on the cells. To determine cell proliferation, the proportion of EdU-labeled cells (red dots) and total DAPI-stained cells (blue dots) was compared. The ImageJ software was used in the quantification of EdU-labeled and DAPI-stained cells.

**Colony formation assay.** To evaluate the capacity of colony formation, we seeded the cells ($1\times10^3$/well) into a six-well plate. Subsequently, the cells were subjected to incubation at 37 °C. On day 14, the culture medium was removed, and the cells were washed with phosphate-buffered saline (PBS). Colonies were immobilized for 20 min at room temperature using a 4% PFA solution. Crystal violet staining (Beyotime) was applied to the colonies for 30 min, followed by PBS wash. The colonies were then photographed and counted using ImageJ software.

**Cell migration and invasion assay.** We conducted migration and invasion experiments by utilizing a 24-well Transwell chamber (Corning, NY, USA), applying a Matrigel coating for the invasion assay and no coating for the migration assay. In the upper chamber, cells ($2\times10^4$/chamber) were seeded in 100 µl of DMEM without FBS, whereas the lower chamber received 550 µl of DMEM with 20% FBS and was incubated at 37 °C for 24 h. Cotton swabs were employed to eliminate cells from the upper chamber; in comparison, the lower membrane-attached cells were treated with 4% PFA solution for 30 min. The cells were subsequently stained with crystal violet for 30 min, visualized under a microscope, and quantified using ImageJ software.

**Immunofluorescence (IF) staining.** The cells ($2\times10^4$/well) were cultured on coverslips overnight in a 24-well plate. Subsequently, the cells were treated with 4% PFA for 15 min. After being fixed in place, the coverslips were permeabilized with 0.1% Triton X-100 for 10 min; thereafter, we proceeded with a 30 min blocking step in 5% BSA. The cells were left to incubate at 4 °C overnight with a primary antibody and then exposed to a fluorescent dye-conjugated secondary antibody (Invitrogen) for 1 h. Finally, fluorescence microscopy was used to examine the coverslips after DAPI staining for 10 min.

**Immunohistochemistry (IHC) staining.** A standard procedure was followed to conduct IHC. The tissues were incubated with a 4% PFA solution, followed by paraffin embedding and subsequent sectioning. The serial sections were then exposed to primary antibodies and left at 4 °C overnight for incubation. Following washing, secondary antibodies were applied to the tissue microarrays for 30 min. Lastly, 5% diaminobenzidine solution (Abcam, Cambridge, USA) was applied for 10 min to induce a brown color.

Two pathologists evaluated the immunohistochemical signals in a double-blinded manner. The proportional scores were as follows: <5% (score 0), 5–25% (score 1), 26–50% (score 2), 51–75% (score 3), and >75% (score 4). The staining intensity was evaluated on a scale of 0 to 3 (0: negative; 1: weak; 2: moderate; 3: strong staining). The formula used to compute the overall score for each slide was as follows: total score = extent score multiplied by intensity score. The primary antibodies used are detailed in Supplementary Table S1.

**Intracranial orthotopic xenografts *in vivo*.** Luciferase-labeled U138 cells ($2\times10^5$/mouse) were implanted into the brains of four-week-old nude male mice (6 mice/group). Bioluminescence imaging was conducted on day 10 and 21 after the intraperitoneal injection of D-luciferin (15 mg/ml) at a dose of 10 µl/g. Harvested intact brains were preserved in 4% PFA, dehydrated, and embedded in paraffin wax for histological examination. The ethics committee of the First Affiliated Hospital of Soochow University granted approval for the experimental protocols (NO.2024480).

**Statistical analysis.** The software tools used to analyze the data were R software (v4.1.3, https://www.r-project.org/) and GraphPad Prism (v8.0, GraphPad Inc., La Jolla, USA). Categorical variables are represented using percentages, whereas continuous variables are reported as the mean ± standard deviation. A p-value <0.05 was deemed to be statistically significant. All quantitative tests were repeated three times in triplicate.

## Results

**IL4I1 expression is upregulated in gliomas and exhibits potential as a molecular marker of malignancy**. Patients with varying levels of IL4I1 expression exhibited distinct clinical and pathological traits. Heatmaps (Figures 1A, 1B) were constructed to display the differential distributions of

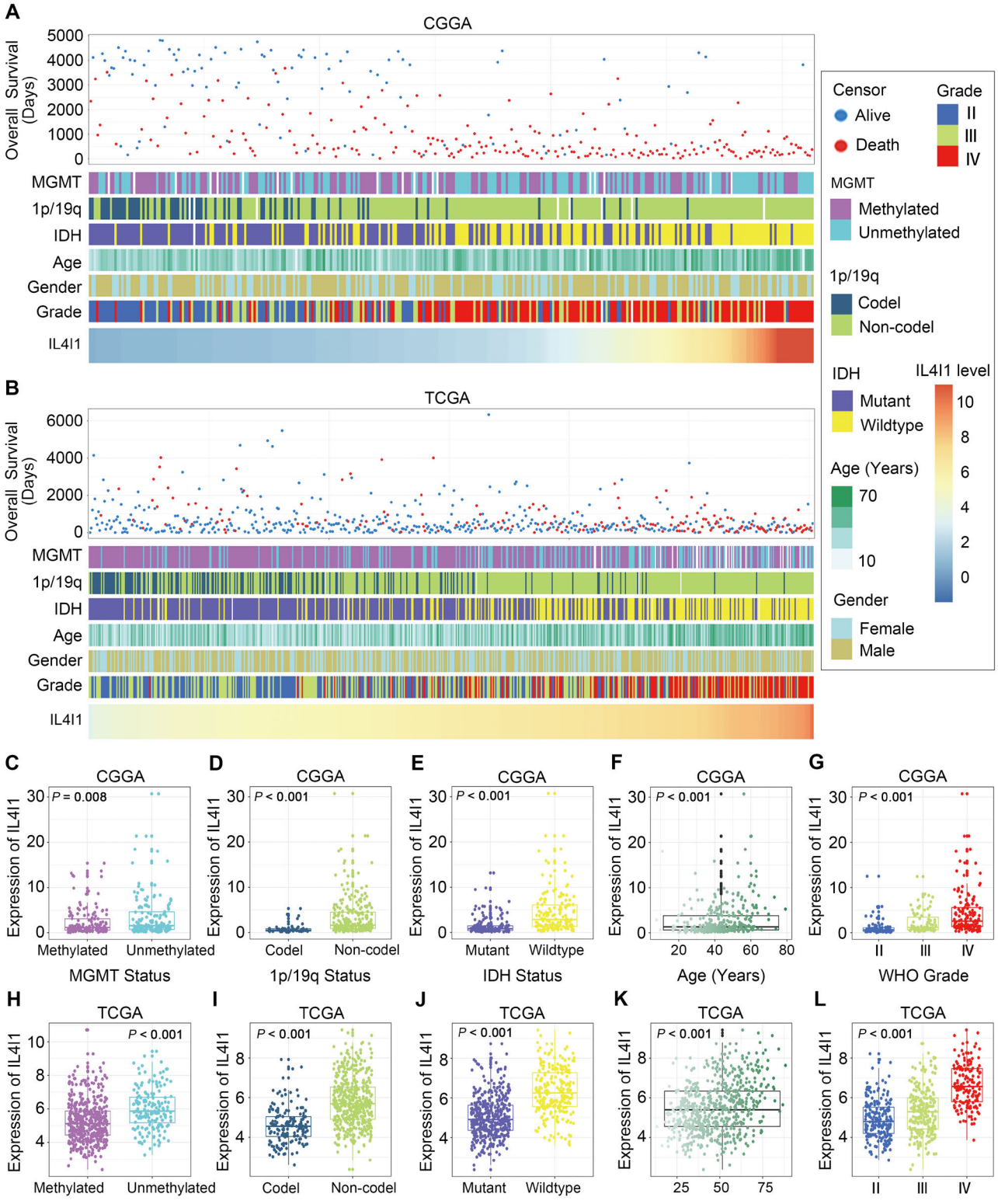


**Figure 1. The association of IL4I1 mRNA level with clinical and pathologic characteristics of gliomas. A, B) The landscape of IL4I1-related clinical and pathologic characteristics of gliomas in CGGA and TCGA cohorts. C–L) Box and scatter plot of relationship between IL4I1 mRNA level and MGMT promoter methylation status (C), 1p/19q status (D), IDH status (E), age (F) and glioma grade (G) in CGGA cohort; and MGMT promoter methylation status (H), 1p/19q status (I), IDH status (J), age (K) and glioma grade (L) in TCGA cohort, respectively. Abbreviations: IL4I1, Interleukin 4-induced gene-1; CGGA, Chinese Glioma Genome Atlas; TCGA, The Cancer Genome Atlas; MGMT, O$^6$-methylguanine-DNA methyltransferase; 1p/19q, chromosome arms 1p and 19q; IDH, isocitrate dehydrogenase**

IL4I1 mRNA expression, $O^6$-methylguanine-DNA methyltransferase (MGMT) promoter methylation, chromosome arms 1p and 19q (1p/19q) codeletion, isocitrate dehydrogenase (IDH) mutation, age, and WHO grade. Subsequently, we performed a comparative analysis of different subgroups of these samples. The association between IL4I1 and the unmethylated MGMT promoter, 1p/19q non-codel, IDH-wildtype, and higher-grade gliomas was significantly pronounced (Figures 1C–1E, 1G, 1H–1J, 1L). Moreover, there was a correlation found between the expression of IL4I1 and increasing age (Pearson $R_{CGGA} = 0.272$; Pearson $R_{TCGA} = 0.339$) (Figures 1F, 1K). To summarize, these findings demonstrate that IL4I1 expression is upregulated in gliomas exhibiting a greater degree of malignancy.

**High IL4I1 expression is correlated with an unfavorable prognosis in glioma patients.** According to data from the Human Protein Atlas (HPA) database (https://www.proteinatlas.org/), IL4I1 exhibited high expression levels in glioma tissues and low expression levels in normal brain tissues (Figure 2A). We examined the clinical characteristics of 76 glioma patients and investigated the relationship between these characteristics and IL4I1 expression using IHC staining. Compared to normal brain tissues, the expression of IL4I1 protein was found to be elevated in glioma tissues of varying grades and showed a positive correlation with the pathological grade of glioma (Figure 2B). Furthermore, the intensity of IL4I1 protein expression was significantly correlated with age and WHO grade but not with gender, tumor location, tumor diameter, or Karnofsky performance status (Supplementary Table S2).

To assess the prognostic significance of IL4I1 in patients with gliomas, we employed Cox proportional hazard models alongside Kaplan-Meier survival analysis by utilizing data from both CGGA and TCGA cohorts. Our multivariate analyses established IL4I1 as an adverse prognostic marker, independent of other well-established prognostic factors (Supplementary Tables S3, S4). The survival analysis results demonstrated significantly lower overall survival (OS) rates in patients in the cohort with elevated IL4I1 expression than in those with lower IL4I1 expression (Figures 2C, 2D). These results indicate that aberrant expression of IL4I1 may be linked to an unfavorable prognosis in human gliomas.

**IL4I1 expression levels in glioma cell lines.** IL4I1 mRNA levels were found to be upregulated to varying degrees in four glioma cell lines (U138, A172, U251, U343) compared to HA1800 human astrocytes using qRT-PCR (Figure 2E). IL4I1 protein levels were elevated in four glioma cell lines (U138, A172, T98, U343) compared to HA1800 human astrocytes using WB (Figure 2F). A172 and U138 cell lines with high IL4I1 expression levels were selected for further analysis.

Moreover, IF staining was employed to assess IL4I1 expression in U138 cell lines. The results showed that IL4I1 was mainly distributed in the cytosolic and perinuclear fractions of U138 cells (Figure 2G).

**IL4I1 knockdown in glioma cell lines.** We established IL4I1-knockdown A172 and U138 cells with lentivirus-mediated shRNAs (sh#1-IL4I1, sh#2-IL4I1, and sh#3-IL4I1). The transfection efficiency was assessed by observing GFP (Figures 3A, 3B). To evaluate the effectiveness of the three shRNA constructs, we measured the expression of IL4I1 mRNA and protein in A172 and U138 cell lines using qRT-PCR (Figure 3C, 3D) and WB (Figures 3E, 3F), respectively. Among them, sh#2-IL4I1 exhibited the highest knockdown efficiency and was selected for further analysis.

**IL4I1 knockdown hampers glioma cell migration, invasion, and proliferation.** The Transwell migration assays revealed notable inhibition of A172 and U138 cell migration in the sh#2-IL4I1 group in contrast with the sh-Ctrl group (Figure 4A). In parallel, the transwell invasion assays yielded similar results (Figure 4B). These findings indicate that IL4I1 knockdown impedes the migratory and invasive abilities of A172 and U138 cells.

The CCK-8 (Figures 4C, 4D) and EdU (Figure 4E) assay results suggested that IL4I1 knockdown suppressed the viability and proliferation of A172 and U138 cells. Colony-forming assays showed that the number of colonies derived from IL4I1-knockdown A172 and U138 cells was significantly reduced (Figure 4F). These results suggest that IL4I1 knockdown effectively suppresses both the proliferation and cell viability of A172 and U138 cells.

**IL4I1 knockdown reverses the EMT process in glioma cells.** The critical role of EMT in many malignant tumor phenotypes, such as migration, invasion, and proliferation, is widely recognized [20, 21]. We next focused on the effects of IL4I1 knockdown on the EMT process.

We individually compared and analyzed the correlation between IL4I1 levels and EMT biomarkers, including epithelial markers (E-cadherin, occludin, desmoplakin, and zonula occludens-1 protein (ZO-1)) and mesenchymal markers (N-cadherin, vimentin, Snail, and Twist1) [13]. The overall correlation of IL4I1 expression is positive with mesenchymal markers and negative with epithelial markers (Figure 5A). Further analysis revealed that IL4I1 exhibited a weaker correlation with E-cadherin and desmoplakin compared to ZO-1 and occludin among the epithelial markers. Additionally, N-cadherin showed less pronounced associations with IL4I1 compared to the other three mesenchymal markers (vimentin, Snail, and Twist1). Both databases showed consistent results.

The WB results indicated that IL4I1 knockdown had a selective impact on EMT-related biomarkers (Figure 5B). Specifically, IL4I1 knockdown resulted in a significant decrease in vimentin expression, accompanied by an increase in ZO-1 expression. IL4I1 knockdown did not exert a discernible impact on the levels of E-cadherin or N-cadherin.

EMT could induce a "cadherin switch", characterized by upregulated N-cadherin and downregulated E-cadherin in the cell membrane, which represents a key hallmark of EMT [22]. Therefore, further study on this progress is warranted.

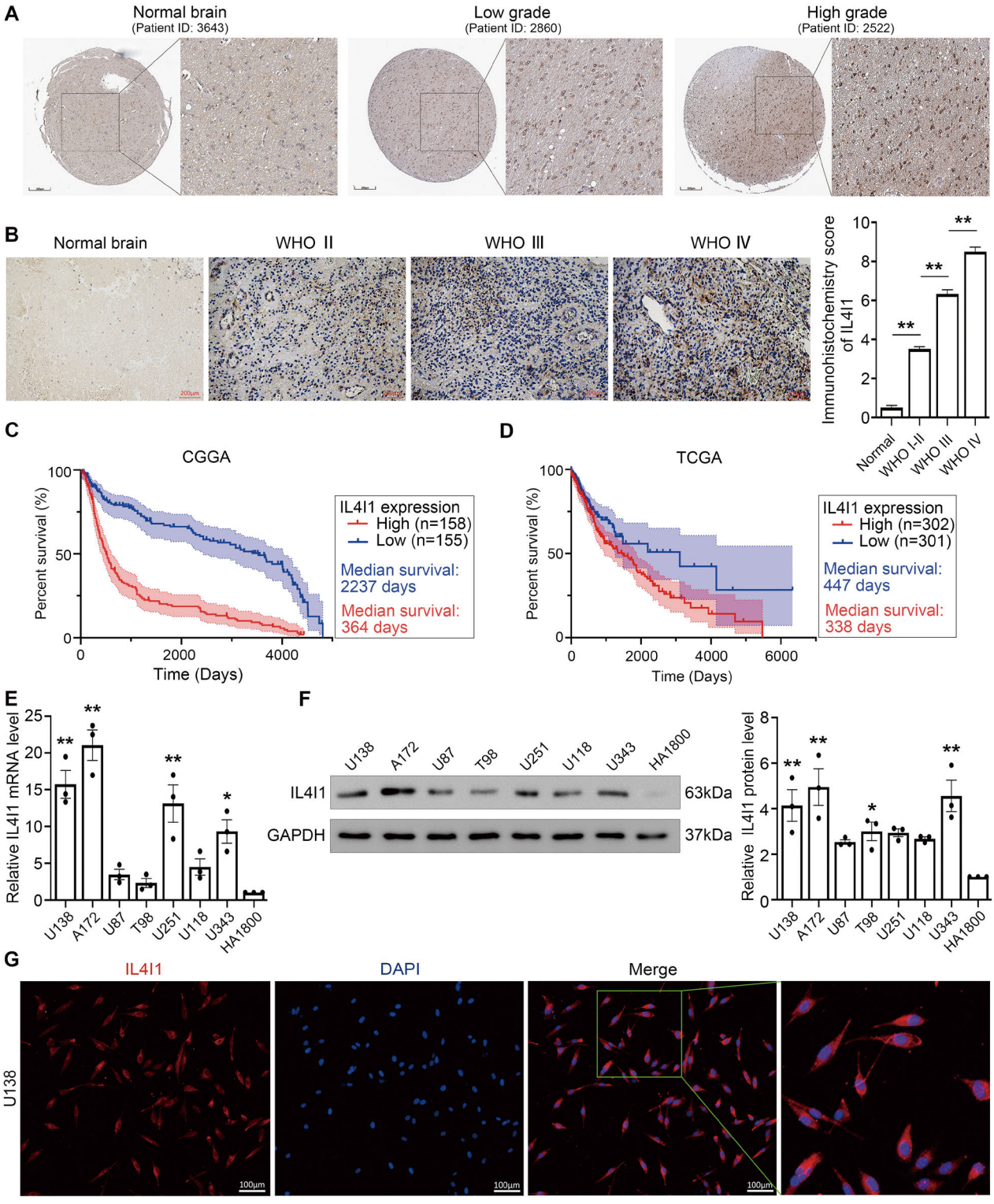


**Figure 2. IL4I1 expression in glioma tissues and cell lines and its prognostic significance in glioma patients. A) Representative IHC staining images of IL4I1 in normal brain, low- and high-grade glioma tissues from the HPA database. B) Representative IHC staining images and score of IL4I1 in normal brain and glioma tissues. C, D) Kaplan-Meier analysis based on IL4I1 expression pattern in CGGA and TCGA cohorts. E) Relative IL4I1 mRNA expression levels in glioma cell lines and a control normal astrocyte cell line HA1800 by real-time quantitative PCR analysis. F) IL4I1 protein expression levels in glioma cell lines and a control normal astrocyte cell line HA1800 by Western blotting analysis. G) Immunofluorescence analysis of IL4I1 (red) and nuclear staining (blue). Quantitative results are presented as the mean ± SEM (n=3). *p<0.05, **p<0.01; Abbreviations: IL4I1-Interleukin 4-induced gene-1; IHC-immunohistochemistry; HPA-Human Protein Atlas; CGGA-Chinese Glioma Genome Atlas; TCGA-The Cancer Genome Atlas**

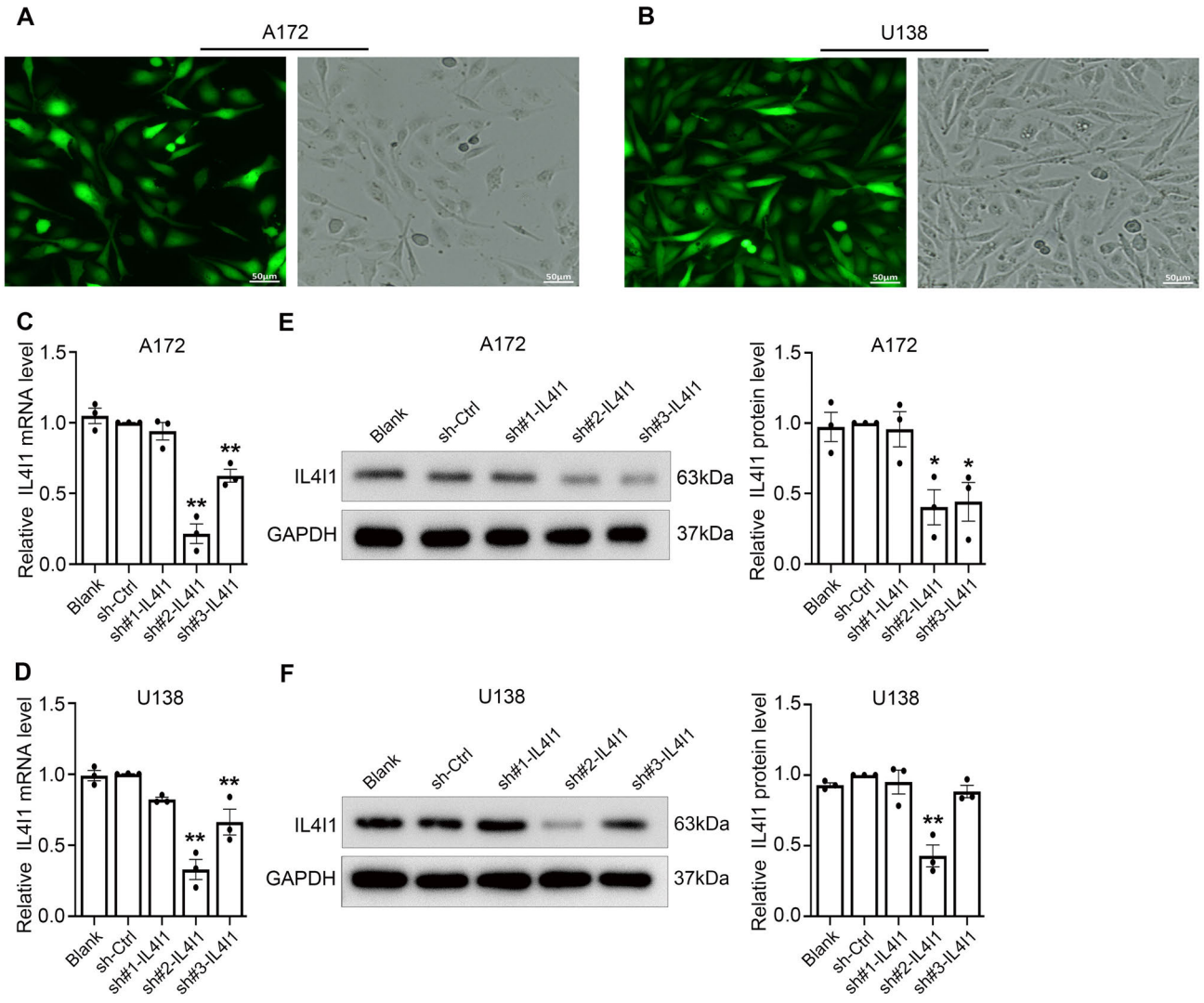


**Figure 3. IL4I1 knockdown in A712 and U138 cell lines. A, B) The transfection efficiency of A712 and U138 cell lines, respectively. C, D) IL4I1 mRNA levels in A712 and U138 cell lines across groups with blank cells, negative control, and IL4I1 knockdown, respectively. E, F) IL4I1 protein levels in A712 and U138 cell lines across groups with blank cells, negative control, and IL4I1 knockdown, respectively. Quantitative results are presented as the mean ± SEM (n=3). *p<0.05, **p<0.01; Abbreviations: IL4I1-interleukin 4-induced gene-1**

Membrane proteins were extracted from A172 and U138 cells using a membrane protein extraction kit. We further examined the changes in membrane levels of E-cadherin and N-cadherin after IL4I1 knockdown in A172 and U138 cell lines using WB. The results showed that IL4I1 knockdown led to an increase in membrane E-cadherin level and a decrease in membrane N-cadherin level (Figure 5C). Combined with the findings from the previous section (Figure 5B), it can be inferred that IL4I1 knockdown did not affect the total cellular levels of E-cadherin and N-cadherin proteins but did alter their respective membrane levels.

Lee et al. emphasized that loss of E-cadherin in the cell membrane is a pivotal process of cancer cell migration and invasion [23]. Then, we analyzed the E-cadherin localization by IF staining. The result visually demonstrated that the E-cadherin location in the sh-Ctrl group was primarily observed in the nuclear fractions, with a minor presence in cytosolic fractions. In contrast, E-cadherin is highly enriched in the cell membrane and reduced in the nuclear fractions following IL4I1 knockdown (Figure 5D).

Overall, the results of these experiments indicate that IL4I1 knockdown partially reverses the EMT process in glioma cells. This reversal is reflected not only in changes in the expression levels of EMT some markers (vimentin and ZO-1), but also in changes in the cellular localization of additional EMT markers (E-cadherin and N-cadherin).

**The JAK2/STAT3 pathway is involved in the IL4I1-mediated EMT process in glioma cells.** The JAK2/STAT3

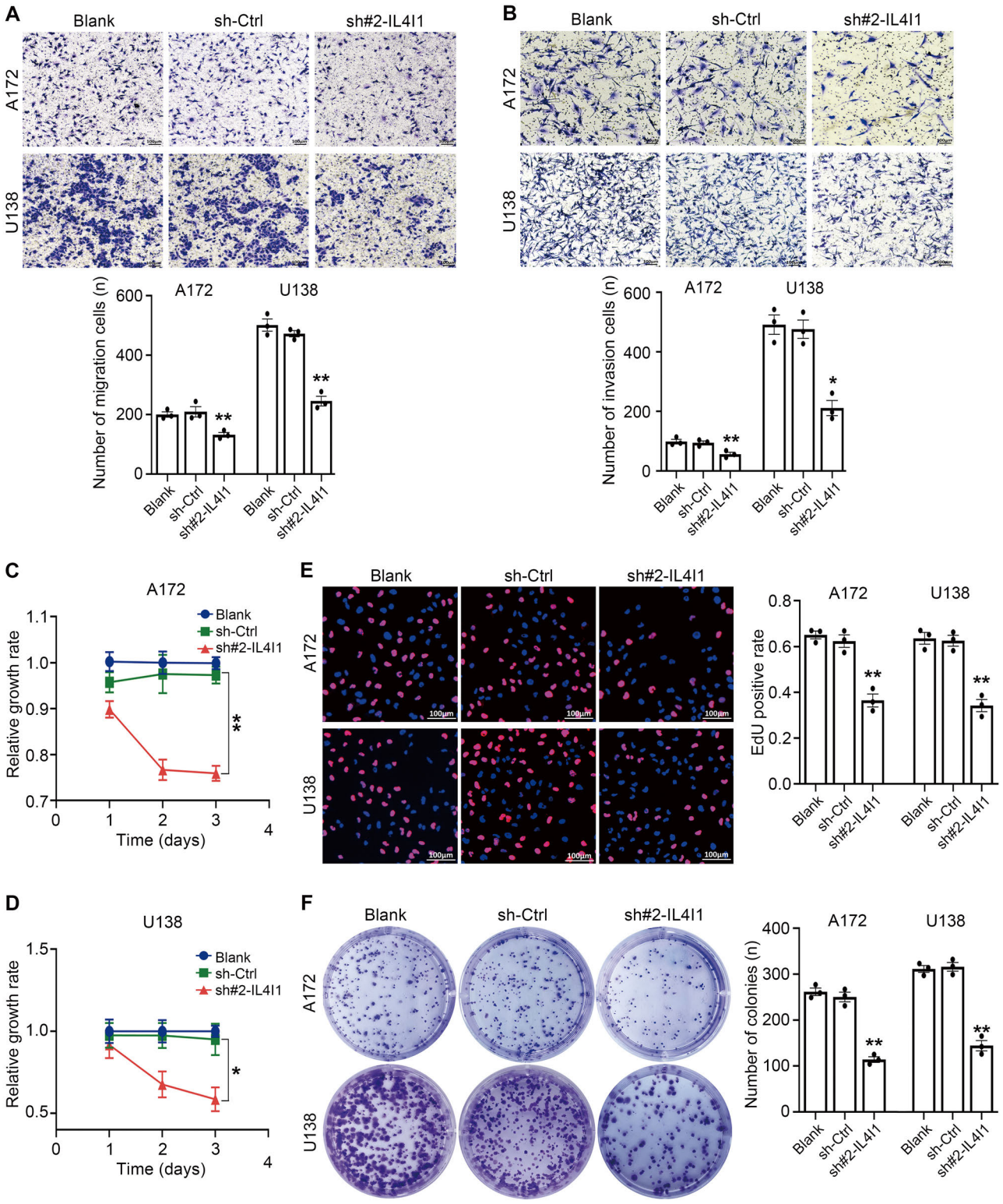


**Figure 4. IL4I1 knockdown inhibits the malignant phenotypes of glioma cells. A) Cell migration assays showing the effects of IL4I1 knockdown on glioma cell migration. B) Cell invasion assays showing the effects of IL4I1 knockdown on glioma cell invasion. C, D) Cell viability was analyzed using CCK-8 assays. E) Cell proliferation was analyzed using EdU assays. F) Colony formation assay was carried out to assess A172 and U138 cells' growth after IL4I1 knockdown for 14 days. Quantitative results are presented as the mean ± SEM (n=3). *p<0.05, **p<0.01; Abbreviations: IL4I1-interleukin 4-induced gene-1; CCK-8-cell counting kit-8; EdU-5-ethynyl-2'-deoxyuridine**

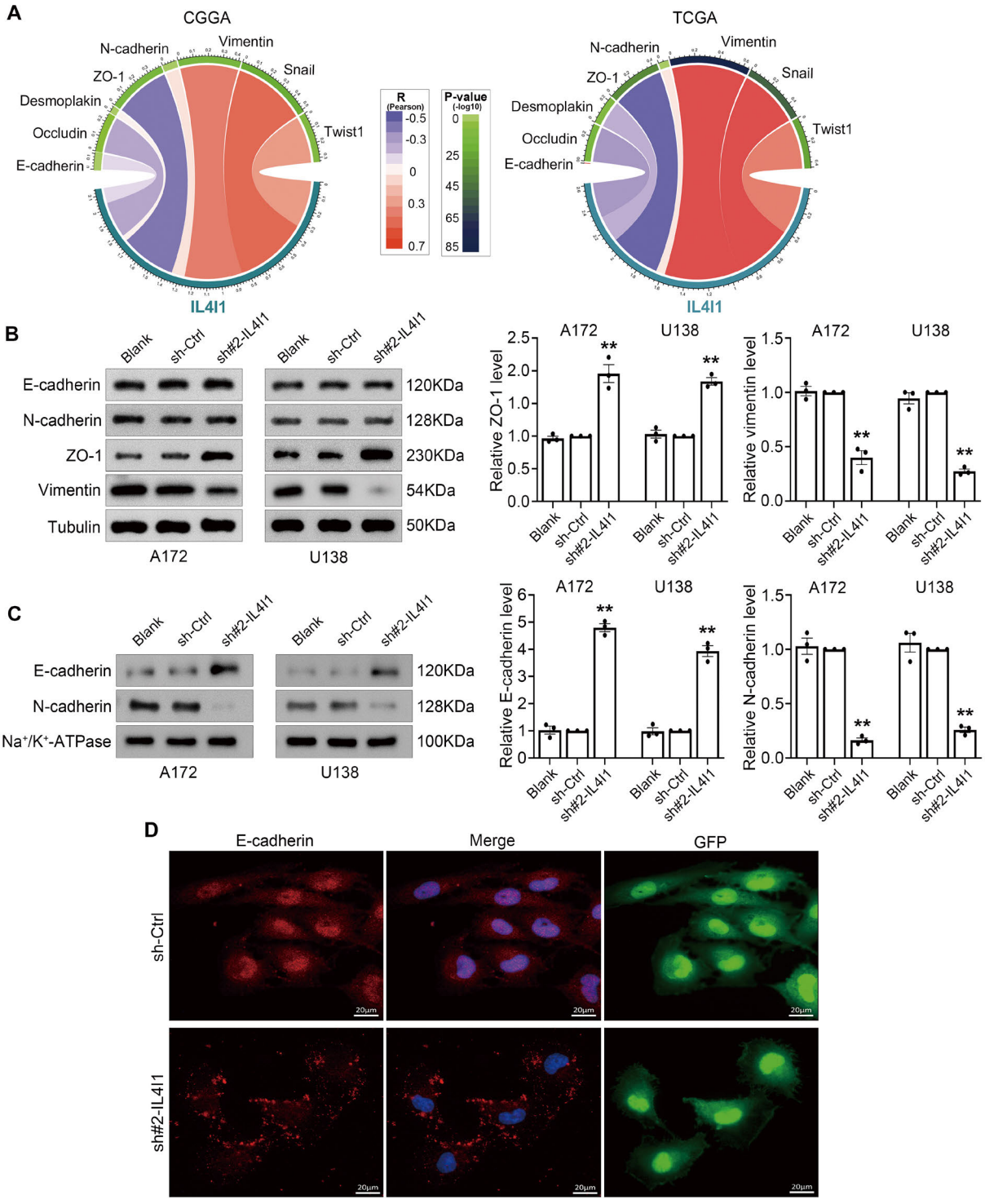


**Figure 5. Effects of IL4I1 knockdown on the EMT process. A) The correlation between IL4I1 and EMT-related biomarkers in CGGA and TCGA cohorts. The width and color of the band in the circle represent the Pearson correlation coefficients. The width and color of the thin band around the circle represent the p-value. B) Western blotting showing changes in the expression of epithelial markers (E-cadherin and ZO-1) and mesenchymal markers (N-cadherin and vimentin) after IL4I1 knockdown. C) Western blotting showing the extracted membrane protein expression of E-cadherin and N-cadherin in each group. After IL4I1 knockdown, membrane E-cadherin level increased while membrane N-cadherin level decreased. D) Immunofluorescence analysis showed that IL4I1 knockdown did not affect the protein expression level of E-cadherin; however, it prompted the distribution of E-cadherin from the nucleus to the cell membrane. Quantitative results are presented as the mean ± SEM (n=3). *p<0.05, **p<0.01; Abbreviations: IL4I1- interleukin 4-induced gene-1; EMT- epithelial-mesenchymal transition; CGGA-Chinese Glioma Genome Atlas; TCGA-The Cancer Genome Atlas**

signaling pathway has been identified as an immensely crucial pathway in driving the malignant phenotypes and EMT of glioma [17, 24]. Our pathway enrichment analysis results showed a significant positive correlation between IL4I1 and the JAK2/STAT3 signaling pathway (Figure 6A).

To investigate whether IL4I1 regulates EMT through the JAK2/STAT3 pathway in A172 and U138 cells, we conducted subsequent experiments. Our WB analysis results showed that IL4I1 knockdown significantly decreased the levels of phosphorylated JAK2 (p-JAK2) and phosphorylated STAT3 (p-STAT3) (Figure 6B). Additionally, downregulation was observed in the relative levels of p-JAK2/JAK2 and p-STAT3/STAT3 in the statistical results (Figure 6B).

To further confirm this finding, we exposed the cells to the JAK2/STAT3 pathway activator (RO8191). The control groups were treated with dimethyl sulphoxide (DMSO). The results revealed that the introduction of RO8191 partially counteracted the impact of IL4I1 knockdown on the phosphorylation of JAK2/STAT3 (Figure 6C). We subsequently found that treatment with RO8191 reduced ZO-1 expression while increasing vimentin expression (Figure 6D). Collectively, the JAK2/STAT3 pathway was found to be involved in IL4I1 knockdown and functionally modulate EMT.

**IL4I1 knockdown impedes glioma progression *in vivo*.** After identifying the impact of IL4I1 knockdown in A172 and U138 cells, we further validated its function *in vivo* (Figure 7A). Bioluminescence imaging data revealed significant inhibition of tumor development in the sh#2-IL4I1 group compared to that in the sh-Ctrl group on day 10 and 21 (Figure 7B).

IHC staining assay of Ki-67 showed that IL4I1 knockdown inhibited cell proliferation *in vivo* (Figure 7C). After IL4I1 knockdown, no changes were observed in the expression levels of E-cadherin and N-cadherin. Nevertheless, an increase in ZO-1 levels and a decrease in vimentin levels were observed (Figure 7D). These findings indicate that, *in vivo*, IL4I1 knockdown in gliomas impedes the tumor burden and reverses the EMT process.

## Discussion

Glioma, originating from glial cell malignant transformation, is a leading cause of mortality among individuals with brain tumors [1, 25]. A major setback with current treatment approaches stems from gliomas' ability to breach the blood-brain barrier and exhibit unlimited proliferative potential [25, 26].

In recent years, IL4I1 has gained recognition as a key regulator of malignant tumor characteristics [5, 9]. A recent comprehensive bioinformatics analysis of IL4I1 also proposed that IL4I1 is firmly related to the poor prognosis of multiple cancers [27]. Our bioinformatics analysis results also indicated that IL4I1 might have a significant impact on intercellular communication and regulation in glioma (Figure 8). Research indicates that increased IL4I1 gene copy numbers in multiple tumor types are associated with unfavorable prognoses [28]. A recent prominent study has proposed that IL4I1 is a novel therapeutic target in cancer [29]. In this study, we examined the effect of IL4I1 knockdown on malignant phenotypes, EMT-related biomarkers, and the underlying mechanism in gliomas. Our findings support the consideration of IL4I1 as a therapeutic target for gliomas.

In the present study, we utilized bioinformatic analysis of data from CGGA and TCGA databases, which encompass extensive clinical samples representing diverse ethnic backgrounds, to explore the expression of IL4I1 in gliomas. Elevated IL4I1 levels are linked to an unfavorable prognosis of human gliomas. Our Cox analysis results also demonstrated that IL4I1 has independent prognostic significance in glioma patients.

Subsequently, through *in vitro* experiments, we confirmed that IL4I1 knockdown effectively hampered the malignant characteristics of glioma cells. Given the role of EMT in dictating the metastatic and invasive behaviors of carcinoma cells, understanding EMT marker alterations is crucial for tumor diagnosis and treatment advancement [21, 30]. Part of the controversy surrounding the EMT process in glioma arises from the developmental origin of glial cells within the neuroepithelial lineage, which exhibit distinct behavior from that of classical epithelial cells [13]. Nonetheless, an EMT process is recognized in brain tumors, and a considerable amount of evidence links EMT to malignant progression and adverse outcomes in gliomas [13, 31].

Through our subsequent experiments, we aimed to elucidate the impact of IL4I1 knockdown on the alterations in EMT-related biomarkers and their underlying molecular pathways. The results revealed that IL4I1 knockdown upregulates ZO-1 expression (an epithelial marker) and downregulates vimentin expression (a mesenchymal marker). In this study, public database analysis and whole-cell lysate WB did not provide evidence for a significant correlation between IL4I1 and E-cadherin or N-cadherin. However, we found that IL4I1 knockdown affected the membrane levels of E-cadherin and N-cadherin, as determined by membrane protein extraction followed by WB analysis. IF staining revealed that changes in the subcellular localization of E-cadherin were evident upon IL4I1 knockdown in U138 cells. The alteration manifested as significantly reduced nuclear staining and increased membranous staining. Similar studies investigating changes in the subcellular localization of E-cadherin have been documented in other tumor types [32, 33]. Therefore, IL4I1 knockdown could still exert an influence on the phenomenon known as the "cadherin switch". The influence is manifested in the changes in the localization of the E-cadherin and N-cadherin. This finding also suggests to us the significance of not solely focusing on alterations in the whole-cell expression levels of the "cadherin switch" but also considering modifications in their intracellular localization when investigating EMT in gliomas.

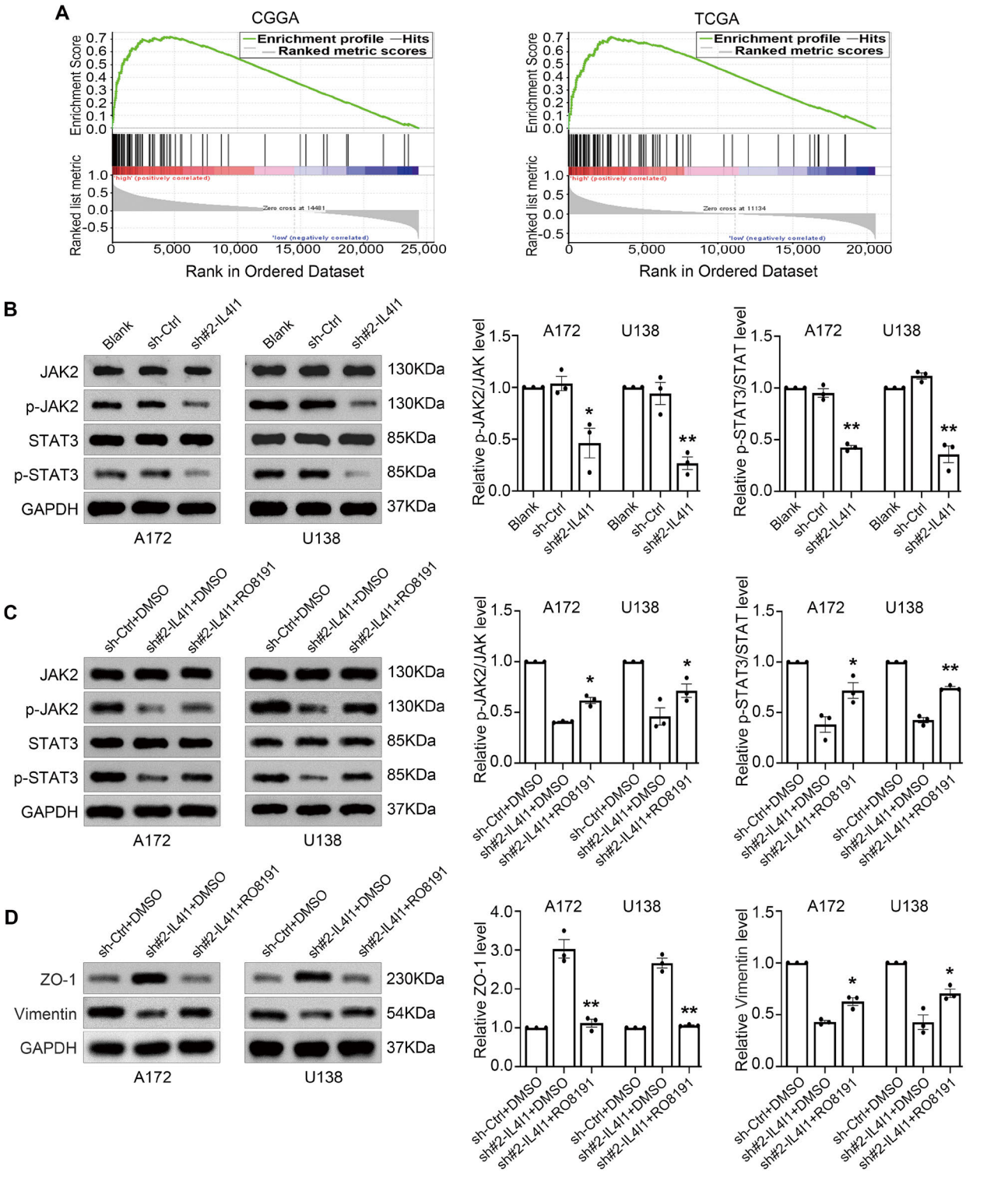


**Figure 6. IL4I1 knockdown inhibits the EMT process by suppressing the JAK2/STAT3 pathway *in vitro*. A) Positive correlation between the JAK2/STAT3 pathway and IL4I1 by GSEA analysis in CGGA and TCGA cohorts. B) The effects of IL4I1 knockdown on the protein levels of the JAK2/STAT3 pathway via Western blotting. C) The addition of RO8191 partially counteracted the effect of IL4I1 knockdown on the JAK2/STAT3 phosphorylation. D) Changes in EMT-related biomarker expression after the JAK2/STAT3 pathway reactivation. Quantitative results are presented as the mean ± SEM (n=3). *p<0.05, **p<0.01; Abbreviations: IL4I1-interleukin 4-induced gene-1; EMT-epithelial-mesenchymal transition; JAK2/STAT3-Janus-activated kinase 2/signal transducer and activator of transcription 3; GSEA-Gene Set Enrichment Analysis; CGGA-Chinese Glioma Genome Atlas; TCGA-The Cancer Genome Atlas**

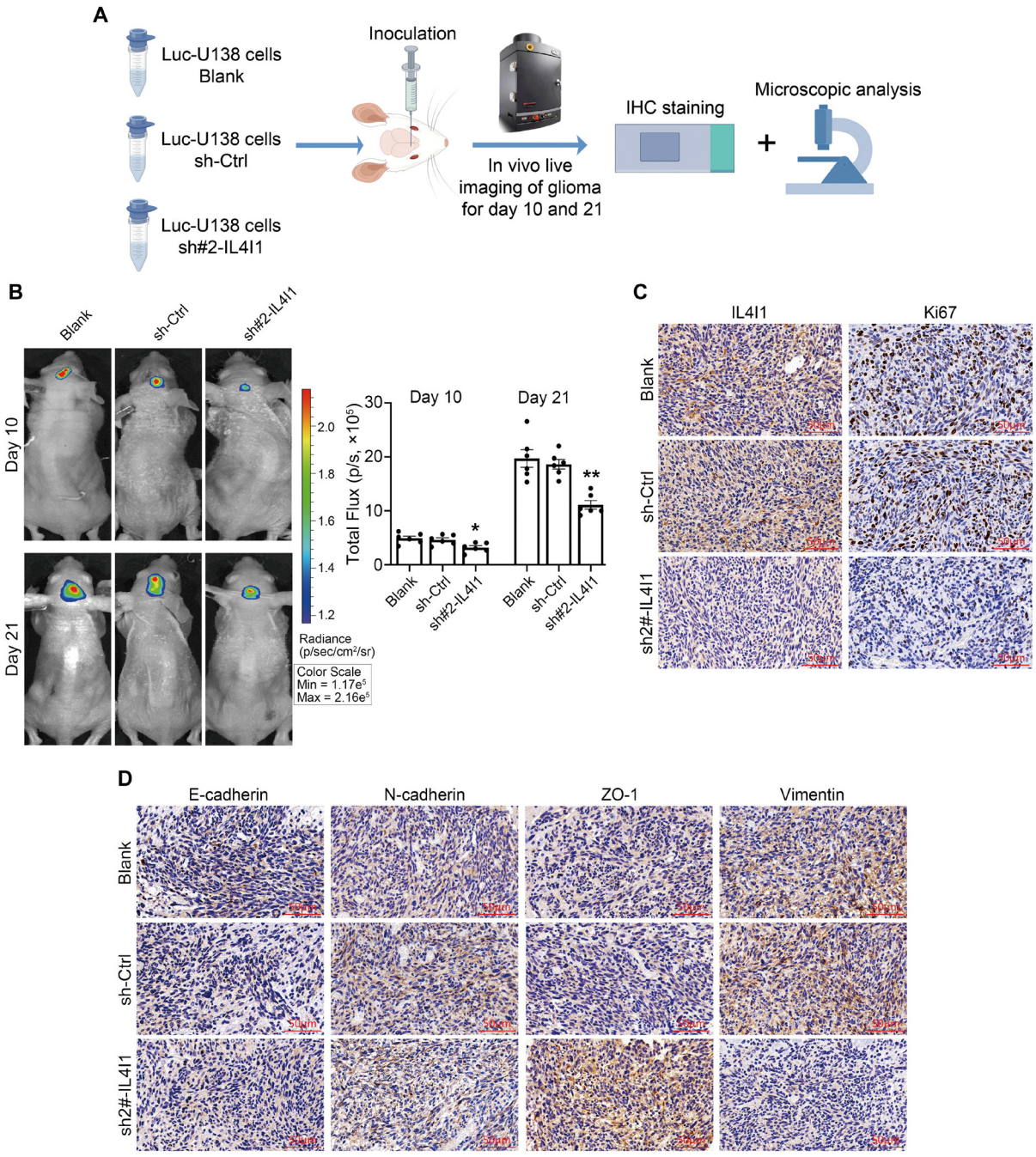


**Figure 7. IL4I1 knockdown suppresses glioma growth, proliferation, and the EMT process *in vivo*. A) Schematic diagram of the xenograft tumor model. B) Representative image and statistical results of tumor-bearing nude mice in each group. C) Representative IHC staining images of IL4I1 and the cell proliferation indicator Ki67 after IL4I1 knockdown. D) Representative IHC staining images of EMT-related biomarker (E-cadherin, N-cadherin, ZO-1, and vimentin) expression after IL4I1 knockdown. Quantitative results are presented as the mean ± SEM (n=6). *p<0.05, **p<0.01; Abbreviations: IL4I1-interleukin 4-induced gene-1; EMT-epithelial-mesenchymal transition; IHC-immunohistochemistry**

The involvement of the JAK2/STAT3 pathway in EMT has been definitively established [17, 34]. In this study, we conducted a more in-depth examination of the correlations among IL4I1, EMT, and the JAK2/STAT3 pathway. Our findings unequivocally demonstrate that IL4I1 knockdown significantly decreases the p-JAK2 and p-STAT3. By introducing RO8191 to rescue the JAK2/STAT3 pathway, we found that IL4I1 modulates the JAK2/STAT3 pathway to hinder the EMT process in glioma cells. Reactivation of the JAK2/STAT3 pathway effectively counteracts the regulatory influ-

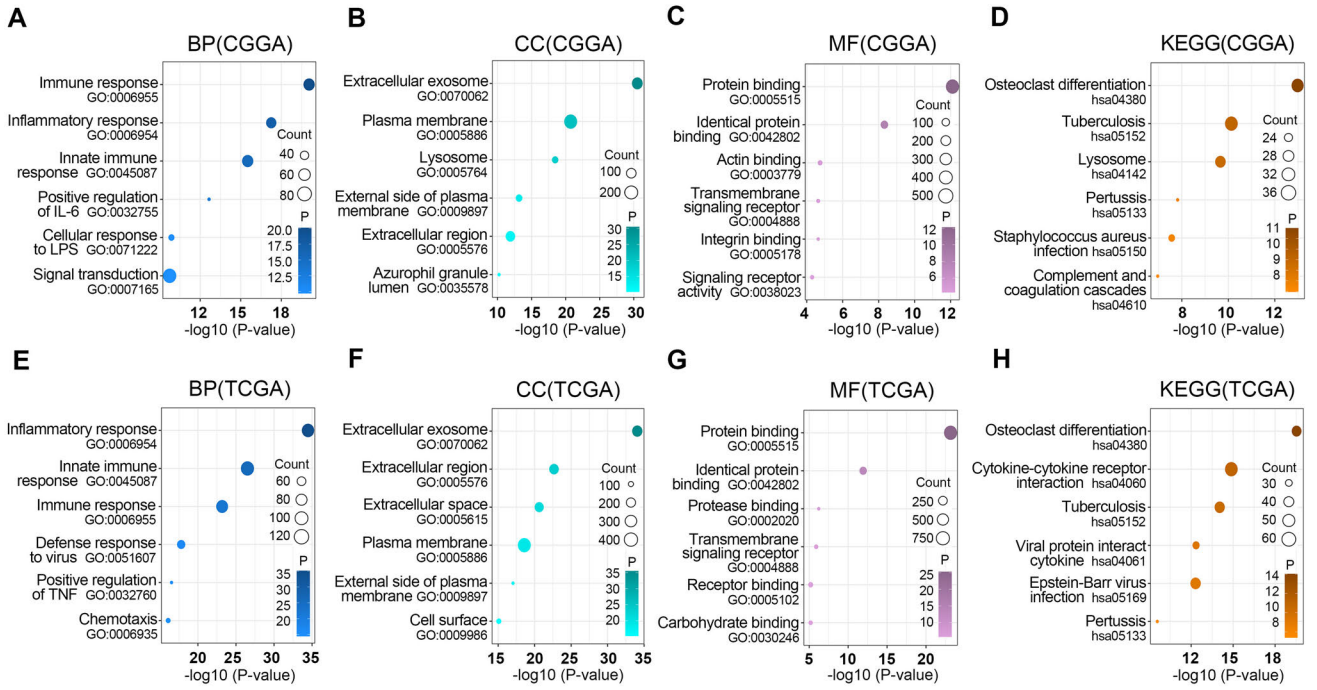


**Figure 8. GO and KEGG enrichment analysis revealed that IL4I1 is closely related to intercellular communication and regulation in glioma. A–C) Significantly enriched GO terms associated with BP, CC, and MF annotations in the CGGA cohort. D) Enrichment analysis of IL4I1-related pathway in the CGGA cohort. E–G) Significantly enriched GO terms associated with BP, CC, and MF annotations in TCGA cohort. H) Enrichment analysis of IL4I1-related pathway in TCGA cohort. Abbreviations: GO-Gene Ontology; KEGG-Kyoto Encyclopedia of Gene and Genomes; IL4I1-interleukin 4-induced gene-1; BP-biological processes; CC-cellular components; MF-molecular functions; CGGA-Chinese Glioma Genome Atlas; TCGA-The Cancer Genome Atlas**

ence of IL4I1 on EMT biomarkers. Furthermore, the results of *in vivo* investigations have indicated that the suppression of IL4I1 inhibits tumor growth. IHC assays indicated that downregulating IL4I1 inhibits tumor cell proliferation and mitigates the EMT process.

Nevertheless, this study is subject to certain constraints. First, the analysis of patients' data was retrospective, based on a limited sample size, and lacked molecular classification. Second, a series of subsequent investigations may be necessary to determine the alterations in the glioma phenotype induced by IL4I1 overexpression and the potential underlying mechanisms involved. Finally, the potential underlying mechanisms by which IL4I1 differentially influences various EMT-biomarkers require further investigation, which is also the focus of our forthcoming research.

To summarize, the research findings indicate the significant upregulation of IL4I1 in glioma, which exhibits a strong correlation with unfavorable patient prognosis. IL4I1 knockdown could inhibit the malignant phenotypes of glioma *in vitro* and *in vivo*. Importantly, we found that IL4I1 knockdown significantly affects the expression levels and localization of EMT-related biomarkers, with this influence being at least partially mediated by the JAK2/STAT3 signaling pathway. Consequently, the findings of this study contribute to a more profound comprehension of the pathogenesis of glioma and the development of therapeutic strategies.

**Supplementary information** is available in the online version of the paper.

Acknowledgments: This work was supported by the Science and Technology Special Fund of Jiangsu Province (Key Research and Development Program for Social Development) (Grant Numbers: BE2023712) and Suzhou Medical Technology Innovation Project-Clinical Frontier (Grant Numbers: SKY2022002). We are profoundly grateful for the invaluable free online databases and resources provided by CGGA, TCGA, and HPA.

## References

[1] LOUIS DN, PERRY A, WESSELING P, BRAT DJ, CREE IA et al. The 2021 WHO classification of tumors of the central nervous system: a summary. Neuro Oncol 2021; 23: 1231–1251. https://doi.org/10.1093/neuonc/noab106

[2] DE ROBLES P, FIEST KM, FROLKIS AD, PRINGSHEIM T, ATTA C et al. The worldwide incidence and prevalence of primary brain tumors: a systematic review and meta-analysis. Neuro Oncol 2015; 17: 776–783. https://doi.org/10.1093/neuonc/nou283

[3] CHIEN LN, OSTROM QT, GITTLEMAN H, LIN JW, SLOAN AE et al. International differences in treatment and clinical outcomes for high-grade glioma. PLoS One 2015; 10: e0129602. https://doi.org/10.1371/journal.pone.0129602

[4] CHU CC, PAUL WE. Fig1, an interleukin 4-induced mouse B cell gene isolated by cDNA representational difference analysis. Proc Natl Acad Sci U S A 1997; 94: 2507–2512. https://doi.org/10.1073/pnas.94.6.2507

[5] BOULLAND ML, MARQUET J, MOLINIER-FRENKEL V, MÖLLER P, GUITER C et al. Human IL4I1 is a secreted L-phenylalanine oxidase expressed by mature dendritic cells that inhibits T-lymphocyte proliferation. Blood 2007; 110: 220–227. https://doi.org/10.1182/blood-2006-07-036210

[6] YUE Y, HUANG W, LIANG J, GUO J, JI J et al. IL4I1 is a novel regulator of M2 macrophage polarization that can inhibit T cell activation via L-tryptophan and arginine depletion and IL-10 production. PLoS One 2015; 10: e0142979. https://doi.org/10.1371/journal.pone.0142979

[7] ZHU J, LI Y, LV X. IL4I1 enhances PD-L1 expression through JAK/STAT signaling pathway in lung adenocarcinoma. Immunogenetics 2023; 75: 17–25. https://doi.org/10.1007/s00251-022-01275-4

[8] MOLINIER-FRENKEL V, PRÉVOST-BLONDEL A, CASTELLANO F. The IL4I1 enzyme: a new player in the immunosuppressive tumor microenvironment. Cells 2019; 8: 757. https://doi.org/10.3390/cells8070757

[9] WANG Z, LI T, MAO C, LIU W, TAO Y. IL4I1-driven AHR signature: a new avenue for cancer therapy. Signal Transduct Target Ther 2021; 6: 118. https://doi.org/10.1038/s41392-021-00529-z

[10] LIU Y, XIANG J, LIAO Y, PENG G, SHEN C. Identification of tryptophan metabolic gene-related subtypes, development of prognostic models, and characterization of tumor microenvironment infiltration in gliomas. Front Mol Neurosci 2022; 15: 1037835. https://doi.org/10.3389/fnmol.2022.1037835

[11] YE F, WANG L, LI Y, DONG C, ZHOU L et al. IL4I1 in M2-like macrophage promotes glioma progression and is a promising target for immunotherapy. Front Immunol 2024; 14: 1338244. https://doi.org/10.3389/fimmu.2023.1338244

[12] TAM WL, WEINBERG RA. The epigenetics of epithelial-mesenchymal plasticity in cancer. Nat Med 2013; 19: 1438–1449. https://doi.org/10.1038/nm.3336

[13] ISER IC, PEREIRA MB, LENZ G, WINK MR. The epithelial-to-mesenchymal transition-like process in glioblastoma: an updated systematic review and in silico investigation. Med Res Rev 2017; 37: 271–313. https://doi.org/10.1002/med.21408

[14] KUBELT C, HATTERMANN K, SEBENS S, MEHDORN HM, HELD-FEINDT J. Epithelial-to-mesenchymal transition in paired human primary and recurrent glioblastomas. Int J Oncol 2015; 46: 2515–2525. https://doi.org/10.3892/ijo.2015.2944

[15] LV S, CHEN Z, MI H, YU X. Cofilin acts as a booster for progression of malignant tumors represented by glioma. Cancer Manag Res 2022; 14: 3245–3269. https://doi.org/10.2147/cmar.S389825

[16] WU H, WEI M, LI Y, MA Q, ZHANG H. Research progress on the regulation mechanism of key signal pathways affecting the prognosis of glioma. Front Mol Neurosci 2022; 15: 910543. https://doi.org/10.3389/fnmol.2022.910543

[17] JIN W. Role of JAK/STAT3 signaling in the regulation of metastasis, the transition of cancer stem cells, and chemoresistance of cancer by epithelial-mesenchymal transition. Cells 2020; 9: 217. https://doi.org/10.3390/cells9010217

[18] PARK J, LEE W, YUN S, KIM SP, KIM KH et al. STAT3 is a key molecule in the oncogenic behavior of diffuse intrinsic pontine glioma. Oncol Lett 2020; 20: 1989–1998. https://doi.org/10.3892/ol.2020.11699

[19] ZHENG X, ZHU Y, WANG X, HOU Y, FANG Y. Silencing of ITGB6 inhibits the progression of cervical carcinoma via regulating JAK/STAT3 signaling pathway. Ann Transl Med 2021; 9: 803. https://doi.org/10.21037/atm-21-1669

[20] WEI J, HUANG K, CHEN Z, HU M, BAI Y et al. Characterization of glycolysis-associated molecules in the tumor microenvironment revealed by pan-cancer tissues and lung cancer single cell data. Cancers (Basel) 2020; 12: 1788. https://doi.org/10.3390/cancers12071788

[21] PARK SY, KORM S, CHUNG HJ, CHOI SJ, JANG JJ et al. RAP80 regulates epithelial-mesenchymal transition related with metastasis and malignancy of cancer. Cancer Sci 2016; 107: 267–273. https://doi.org/10.1111/cas.12877

[22] ZEISBERG M, NEILSON EG. Biomarkers for epithelial-mesenchymal transitions. J Clin Invest 2009; 119: 1429–1437. https://doi.org/10.1172/jci36183

[23] LEE YS, KIM SY, SONG SJ, HONG HK, LEE Y et al. Crosstalk between CCL7 and CCR3 promotes metastasis of colon cancer cells via ERK-JNK signaling pathways. Oncotarget 2016; 7: 36842–36853. https://doi.org/10.18632/oncotarget.9209

[24] ZHANG P, CHEN FZ, JIA QB, HU DF. Upregulation of microRNA-133a and downregulation of connective tissue growth factor suppress cell proliferation, migration, and invasion in human glioma through the JAK/STAT signaling pathway. IUBMB Life 2019; 71: 1857–1875. https://doi.org/10.1002/iub.2126

[25] OSTROM QT, GITTLEMAN H, TRUITT G, BOSCIA A, KRUCHKO C et al. CBTRUS statistical report: primary brain and other central nervous system tumors diagnosed in the United States in 2011–2015. Neuro Oncol 2018; 20: iv1–iv86. https://doi.org/10.1093/neuonc/noy131

[26] XUE T, DING JS, LI B, CAO DM, CHEN G. A narrative review of adjuvant therapy for glioma: hyperbaric oxygen therapy. Med Gas Res 2021; 11: 155–157. https://doi.org/10.4103/2045-9912.318861

[27] CHEN B, LIU Y, HE Y, SHEN C. Pan-cancer analysis of prognostic and immunological role of IL4I1 in human tumors: a bulk omics research and single cell sequencing validation. Discov Oncol 2024; 15: 139. https://doi.org/10.1007/s12672-024-01000-5

[28] CARBONNELLE-PUSCIAN A, COPIE-BERGMAN C, BAIA M, MARTIN-GARCIA N, ALLORY Y et al. The novel immunosuppressive enzyme IL4I1 is expressed by neoplastic cells of several B-cell lymphomas and by tumor-associated macrophages. Leukemia 2009; 23: 952–960. https://doi.org/10.1038/leu.2008.380

[29] SADIK A, SOMARRIBAS PATTERSON LF, ÖZTÜRK S, MOHAPATRA SR, PANITZ V et al. IL4I1 is a metabolic immune checkpoint that activates the AHR and promotes tumor progression. Cell 2020; 182: 1252–1270. https://doi.org/10.1016/j.cell.2020.07.038

[30] PASTUSHENKO I, BLANPAIN C. EMT transition states during tumor progression and metastasis. Trends Cell Biol 2019; 29: 212–226. https://doi.org/10.1016/j.tcb.2018.12.001

[31] MAHABIR R, TANINO M, ELMANSURI A, WANG L, KIMURA T et al. Sustained elevation of Snail promotes glial-mesenchymal transition after irradiation in malignant glioma. Neuro Oncol 2014; 16: 671–685. https://doi.org/10.1093/neuonc/not239

[32] CHUNG VY, TAN TZ, TAN M, WONG MK, KUAY KT et al. GRHL2-miR-200-ZEB1 maintains the epithelial status of ovarian cancer through transcriptional regulation and histone modification. Sci Rep 2016; 6: 19943. https://doi.org/10.1038/srep19943

[33] PINHO SS, REIS CA, PAREDES J, MAGALHÃES AM, FERREIRA AC et al. The role of N-acetylglucosaminyltransferase III and V in the post-transcriptional modifications of E-cadherin. Hum Mol Genet 2009; 18: 2599–2608. https://doi.org/10.1093/hmg/ddp194

[34] YEH CT, CHEN TT, SATRIYO PB, WANG CH, WU ATH et al. Bruton's tyrosine kinase (BTK) mediates resistance to EGFR inhibition in non-small-cell lung carcinoma. Oncogenesis 2021; 10: 56. https://doi.org/10.1038/s41389-021-00345-8

https://doi.org/10.4149/neo_2025_250110N13

# IL4I1 knockdown inhibits the epithelial-mesenchymal transition process in glioma via downregulation of the JAK2/STAT3 signaling pathway

Jianwei ZHUO[1,2,#], Tong WANG[1,#], Ting LU[1], Xiangying LI[1], Zhengquan YU[1], Gang CUI[1,*], Haitao SHEN[1,*]

## Supplementary Information

**Supplementary Table S1. Primary antibodies used in this research.**

| Antibody name | Species | Vendor | Catalog number |
|---|---|---|---|
| IL4I1 | Rabbit | Affinity Biosciences | DF4819#311 |
| E-cadherin | Mouse | ProteinTech | 60335-1-lg |
| N-cadherin | Rabbit | ProteinTech | 22018-1-AP |
| ZO-1 | Mouse | ProteinTech | 66452-1-lg |
| Vimentin | Rabbit | ProteinTech | 10366-1-AP |
| JAK2 | Rabbit | Affinity Biosciences | AF6022 |
| p-JAK2 | Rabbit | Affinity Biosciences | AF3024 |
| STAT3 | Rabbit | Affinity Biosciences | AF6294 |
| p-STAT3 | Rabbit | Affinity Biosciences | AF3293 |
| Ki67 | Rabbit | ProteinTech | 27309-1-AP |

**Supplementary Table S2. Association of IL4I1 expression with the clinical parameters in gliomas.**

| Parameter | Total | L4I1 expression | | |
|---|---|---|---|---|
| | | Low | High | p-value |
| Total | 76 | 35 (46.1%) | 41(53.9%) | |
| Gender | | | | 0.193 |
| Male | 33 | 18 (51.4%) | 15 (36.6%) | |
| Female | 43 | 17 (48.6%) | 26 (63.4%) | |
| Age (year) | 76 | 41.26±11.56 | 47.5±11.68 | 0.022 |
| WHO grade | | | | 0.003 |
| Low-grade (I–II) | 36 | 23 (65.7%) | 13 (31.7%) | |
| High-grade (III–IV) | 40 | 12 (34.3%) | 28 (68.3%) | |
| Tumor location | | | | 0.375 |
| Temporal | 28 | 15 (42.9%) | 13 (31.7%) | |
| Frontal | 37 | 14 (40.0%) | 23 (56.1%) | |
| Other | 11 | 6 (17.1%) | 5 (12.2%) | |
| Tumor diameter (cm) | | | | 0.960 |
| ≤4 | 28 | 13 (37.1%) | 15 (36.6%) | |
| >4 | 48 | 22 (62.9%) | 26 (63.4%) | |
| KPS score | | | | 0.278 |
| <80 | 34 | 18 (51.4%) | 16 (39.0%) | |
| ≥80 | 42 | 17 (48.6%) | 25 (61.0%) | |

Abbreviation: IL4I1 – interleukin 4-induced gene-1; KPS – Karnofsky performance status

**Supplementary Table S3. Univariate and multivariate analysis of prognostic parameters for overall survival (OS) in Chinese Glioma Genome Atlas (CGGA) cohort.**

| Parameter | Univariate analysis | | Multivariate analysis | |
|---|---|---|---|---|
| | HR (95% CI) | p-value | HR (95% CI) | p-value |
| MGMT status | 0.830 (0.632–1.089) | 0.178 | | |
| 1p/19q codel | 0.170 (0.104–0.277) | <0.001 | 0.229 (0.137–0.385) | <0.001 |
| IDH status | 0.355 (0.269–0.468) | <0.001 | 1.080 (0.776–1.504) | 0.648 |
| Age | 1.033 (1.020–1.046) | <0.001 | 1.014 (1.002–1.027) | 0.020 |
| Gender | 0.941 (0.716–1.236) | 0.660 | | |
| WHO grade* | 5.657 (3.917–8.171) | <0.001 | 4.273 (2.889–6.321) | <0.001 |
| IL4I1 expression | 1.093 (1.067–1.118) | <0.001 | 1.043 (1.012–1.074) | 0.005 |

Note: *WHO grade I and II gliomas were classified as low-grade, and WHO grade III and IV gliomas were classified as high-grade. Abbreviations: CI – confidence interval; HR – hazard ratio; MGMT – $O^6$-methylguanine-DNA methyltransferase; 1p/19q – chromosome arms 1p and 19q; IDH – isocitrate dehydrogenase; IL4I1 – interleukin 4-induced gene-1

**Supplementary Table S4. Univariate and multivariate analysis of prognostic parameters for overall survival (OS) in The Cancer Genome Atlas (TCGA) cohort.**

| Parameter | Univariate analysis | | Multivariate analysis | |
|---|---|---|---|---|
| | HR (95% CI) | p-value | HR (95% CI) | p-value |
| MGMT status | 0.312 (0.225–0.433) | <0.001 | 0.902 (0.613–1.328) | 0.602 |
| 1p/19q codel | 0.220 (0.130–0.375) | <0.001 | 0.533 (0.283–1.004) | 0.051 |
| IDH status | 0.091 (0.064–0.129) | <0.001 | 0.343 (0.200–0.590) | <0.001 |
| Age | 1.075 (1.063–1.088) | <0.001 | 1.060 (1.045–1.075) | <0.001 |
| Gender | 1.001 (0.743–1.347) | 0.997 | | |
| WHO grade* | 6.103 (3.890–9.574) | <0.001 | 2.259 (1.356–3.763) | 0.002 |
| IL4I1 expression | 1.805 (1.613––2.020) | <0.001 | 1.206 (1.044–1.392) | 0.011 |

Note: *WHO grade I and II gliomas were classified as low-grade, and WHO grade III and IV gliomas were classified as high-grade. Abbreviations: CI – confidence interval; HR – hazard ratio; MGMT – $O^6$-methylguanine-DNA methyltransferase; 1p/19q – chromosome arms 1p and 19q; IDH – isocitrate dehydrogenase; IL4I1 – interleukin 4-induced gene-1